03,10

Unravelling the band structure features of HgTe nanoplatelets in ultrathin limit

© V.G. Kuznetsov[1], A.A. Gavrikov[2], A.V. Kolobov[2]

[1] Ioffe Institute,
St. Petersburg, Russia
[2] Herzen State Pedagogical University of Russia,
St. Petersburg, Russia

E-mail: vladimir.kuznetsov@mail.ioffe.ru

Received September 16, 2025
Revised October 26, 2025
Accepted November 6, 2025

The band structure of mercury telluride (HgTe) nanoplatelets in the two-monolayer (2ML) limit was studied taking into account spin-orbit coupling and using various density functional theory (DFT) types. Single-layer (1ML) and two-layer (2ML) HgTe nanoplatelets in the sphalerite phase, as well as bulk HgTe, were considered. It was demonstrated that strong spin-orbit coupling, combined with two-dimensional quantum confinement, lead to significant changes in the electronic band structure of ultrathin two-dimensional (2D) HgTe nanoplatelets and the ordering of their boundary bands compared to a three-dimensional material. Calculations of band structure of 2D-nanoplatelets in ultrathin limit revealed a number of specific features: (i) the nature of band structure of 1ML-HgTe (inverted/non-inverted band order) depends on the type of density functional used; (ii) the regular band structure of 1ML-HgTe has a non-inverted (normal) band order, and the nanoplatelet itself is a direct-gap semiconductor at the Γ point; (iii) the band structure of 2ML-HgTe has no forbidden band and has an inverted band order; (iv) the band structure of 2ML-HgTe near the Fermi level exhibits behavior characteristic of a type II Weyl semimetal.

Keywords: mercury telluride, 2D-nanoplatelets, inverted band structure, type II Weyl semimetal.

DOI: 10.61011/PSS.2025.11.62953.255-25

1. Introduction

Two-dimensional (2D) materials are of great interest both from the fundamental point of view and for rational design of microelectronic devices with new functional capabilities within the atomically thin limit. Material thickness reduction usually results in changes in various properties and appearance of new interesting features in the electronic structure. Discovery of graphene [1] has led to an explosive interest in searching for other 2D-materials that are critical for various applications in optoelectronics, spintronics, solar power engineering [2,3] etc.

Most 2D-materials, such as hexagonal boron nitride (h-BN), chalcogenides of metals, transition metal dichalcogenides, are made of three-dimensional (3D) layered structures by mechanical or chemical exfoliation of individual layers. The exfoliation process is facilitated by the fact that individual layers with a strong covalent bonding within the layer are held together by weak van der Waals forces. Besides, apart from layered 3D-materials there are some, such as, for example, silicene and germanene, which have stable 2D-structures and a wide spectrum of interesting properties. Silicene was theoretically predicted by [4–9] as a buckled honeycomb structure from silicon atoms (Si), having electron dispersion specific for Dirac's cone. Silicene was successfully grown on Ag [10–13], Ir [14] and ZrB_2 [15] substrates and is considered by many to be as one of the most promising materials for next generation electronic devices [7,9,12].

Mercury chalcogenides HgX ($X =$ S, Se, Te) stand out among the materials of the group A^{II}-B^{VI} by their unusual physical properties, caused by a gapless band structure and, accordingly, the absence of the energy threshold for production of electron-hole pairs. Gapless mercury telluride (HgTe) can be considered [16] simultaneously as a semiconductor without a band gap and a metal without free electrons at $T = 0$ K. On the other hand, one may consider HgTe either a semiconductor with an empty conduction band and adjacent completely filled valence band or a metal with a half-filled band, but with zero density of states at Fermi level [16].

In bulk HgTe the states of the valence 6-fold degenerate (with account of spin) p-band, corresponding to the irreducible representation (IR) Γ_{15}, with account of spin-orbit coupling, are split into 4-fold degenerate bands Γ_8 of heavy and light holes and 2-fold degenerate spin-orbit split band Γ_7. Besides, the conduction band Γ_6, specific for bulk cadmium telluride (CdTe), with s-type symmetry, in the HgTe crystals turns out to be lower by energy of valence band Γ_8, as the calculations with the $\mathbf{k}\cdot\mathbf{p}$-method show [17]. As a result, the width of the band gap of bulk HgTe at $T = 0$ K, defined as $E_g = E(\Gamma_6) - E(\Gamma_8)$, turns out to be negative (-0.28 eV) [17]. Experiments of photo-emission with angular resolution demonstrated that

E_g for HgTe has negative values, namely, -0.29 ± 0.02 eV at temperature of 40 K and -0.32 ± 0.03 eV at 300 K [18]. Besides, the value of the spin-orbit splitting turns out to be equal to 0.91 eV, which substantially exceeds the corresponding value for CdTe [18]. Strong spin-orbit coupling in the HgTe crystal provides for the inverse order of band structure ($\Gamma_7-\Gamma_6-\Gamma_8$), compared to CdTe band structure ($\Gamma_7-\Gamma_8-\Gamma_6$). The inverse band structure of bulk HgTe is a unique property that is critical for implementation of the quantum spin Hall effect in quantum 2D-wells of HgTe/CdTe, in which the HgTe layer is between two CdTe layers [19–21].

The important feature of HgTe and other materials of the A^{II}-B^{VI} group is also the possibility to synthesize the 2D-structures that are nanoplatelets with thickness from one to several monolayers (ML). Besides, a monolayer means a quasi-two-dimensional plate made of two planes, one formed with metal atoms ($Me =$ Zn, Cd, Hg), and the other one — with chalcogen atoms ($X =$ S, Se, Te). The synthesis of 2D-structures opens the possibilities to control physical properties of the material by changing the thickness [22–24]. In particular, it is known that the reduction of the number of monolayers causes the increased width of the band gap in the semiconductors as a result of quantum-size effects [25].

The purpose of this paper is the theoretical study of the band structure features in HgTe nanoplatelets in the sphalerite phase in the limit of two MLs. These features are due to strong spin-orbit coupling in a combination with two-dimensional quantum confinement, which causes substantial changes in the band structure of ultrathin HgTe 2D-nanoplatelets and ordering of their boundary bands compared to a 3D-material having the inverse band structure.

2. Computational details

The calculations were carried out with account of spin-orbit coupling by the density functional theory (DFT) method in GGA and GGA+U approximations with GGA-functional in the form of PBEsol [26] using a plane wave code Quantum Espresso (QE) [27,28]. Hubbard repulsion was taken into account by two different methods: (i) in the Liechtenstein formulation $U-J$, which includes not only the Hubbard's correction U, but also the Hund's correction J [29]; (ii) in the simplified (rotational-invariant) Dudarev's formulation, where instead of U and J separately only one effective parameter is considered: $U_{\text{eff}} = U - J$ (lower index eff is often omitted) [30]. To describe the electron-ion interactions, fully relativistic (j-dependent) PAW (Projector Augmented-Wave) potentials were used [31] from the library of pseudopotentials of the QE code (psl 1.0.0) [32]. The $6s^25d^{10}$-electrons of Hg atoms and $5s^25p^4$-electrons of Te atoms were considered as valence ones.

Complete relaxation of all structures was carried out using so called BFGS (Broyden–Fletcher–Goldfarb–Shanno) algorithm [33–36]. Atomic positions and the cell parameters were optimized until the differences of energies, Hellmann-Feynman forces on the atoms and pressure did not decrease down to values $1 \cdot 10^{-10}$ Ry, $1 \cdot 10^{-6}$ Ry $\cdot$ r_B^{-1} (where r_B — Bohr radius), $1 \cdot 10^{-2}$ kbar respectively. The process of self-consistency for each fixed geometry stopped when the energy discrepancy was $1 \cdot 10^{-12}$ Ry. In the plane wave basis expansion the kinetic energy $E_{\text{cutoff}} = 80$ Ry was used. When integrating over the Brillouin zone for bulk HgTe the Monkhorst–Pack [37] **k**-mesh $9\times9\times9$ was used (35 **k**-points in the irreducible part of the Brillouin zone (IBZ)). For 1ML- and 2ML-HgTe nanoplatelets in sphalerite phase the **k**-meshs of $8\times8\times3$ were chosen (25 **k**-points in IBZ). The used **k**-samplings for bulk HgTe and HgTe nanoplatelets were selected in the concerted manner so that the corresponding distances between the **k**-points were approximately the same and did not exceed the values 0.03 Å^{-1}, which corresponds approximately to the same accuracy of calculations.

Such strict tolerance values and E_{cutoff} were selected with account of the fact that the subsequent calculations of phonon dispersion require finding the equilibrium geometry with very high accuracy. Calculations of vibrational states and dispersion of phonons of ultrathin 2D-nanoplatelets with account of spin-orbit coupling were performed by us for a fully optimized geometry by two different methods, usually used to calculate the phonons based on the first principles: approximation of linear response within the density functional perturbation theory (DFPT) [38–46] and the finite-displacement supercell approach (FDSA) [47]. Besides, for the phonon calculations performed by DFPT method we used the implementation of the density functional perturbation theory adapted for 2D-structures, suggested in paper [48] and implemented into plane wave code Quantum Espresso [27,28]. This implementation of the DFPT method for 2D-structures takes into account the circumstance that the traditionally used approaches with three-dimensional periodic boundary conditions are not quite suitable to simulate two-dimensional materials. This is mainly due to the fact [48] that in response to long-wavelength perturbations, parasite interaction appears between the system and the off-plane periodical images caused by behavior of the $\propto 1/q^2$ Fourier transform of the three-dimensional Coulomb potential. To eliminate this artifact, it is proposed [48] to include the truncated Coulomb interaction in the direction perpendicular to the plate, which usually makes it possible to avoid the appearance of imaginary acoustic frequencies near the point Γ.

Verification calculations of phonon dispersion within the FDSA approach [47] were performed using Phono3py code [49,50].

3. Results and discussion

The study of the electron structure of the 2ML-HgTe nanoplatelet was preceded by the examination of the 1ML-HgTe nanoplatelet with the zigzag-shaped structure

(low-buckled), which is a monolayer of two atomic planes of Hg and Te, shifted from each other by value Δ (Figure 1). As a result of complete structural relaxation of the zigzag-shaped nanoplatelet 1ML-HgTe by the DFT method, the lattice constant turned out to be equal to 4.649 Å, and the bend value Δ — 0.465 Å, which agrees well with the values 4.616 and 0.470 Å from paper [51] with account of differences in the used functionals and pseudopotentials.

In this paper, except for 1ML-HgTe nanoplatelet, 2ML-HgTe nanoplatelet was also considered with sphalerite structure. Both nanoplatelets were built by cleavage of bulk HgTe (Figure 2, *a*) along the surface (111). 2ML-HgTe nanoplatelet consisting of two monolayers has the sequence of atomic planes Te–Hg–Te–Hg, as shown in Figure 2, *b*. For the 2ML-HgTe nanoplatelet, fully relaxed by the DFT method, the lattice constant value of 4.636 Å was obtained.

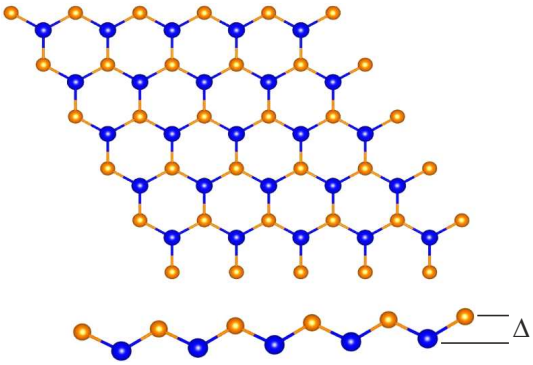

Figure 1. Top and side view of 1ML-HgTe zigzag-like monolayer, where Δ — monolayer bend value (distance between Te and Hg atom planes). Hg atoms are shown in blue, Te atoms — in orange.

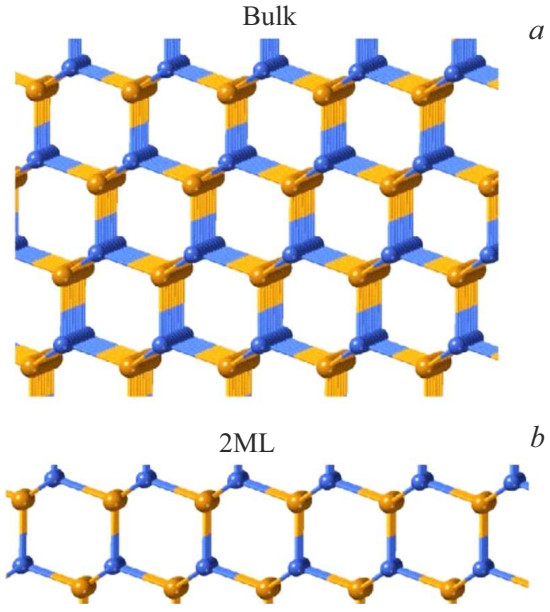

Figure 2. *a*) bulk HgTe, *b*) 2ML-HgTe. Hg atoms are shown in blue, Te atoms — in orange.

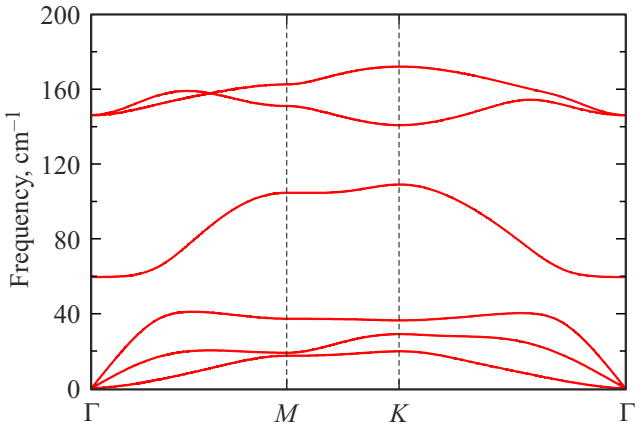

Figure 3. Dispersion of phonon branches for 1ML-HgTe nanoplatelet.

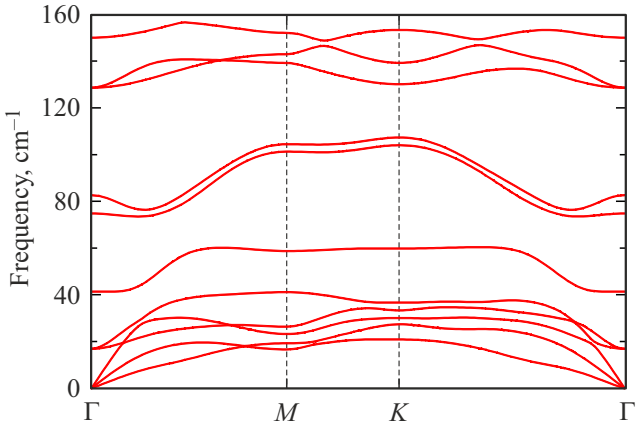

Figure 4. Dispersion of phonon branches for 2ML-HgTe nanoplatelet.

For both relaxed ultrathin HgTe nanoplatelets, we used QE code[27,28] to perform DFPT-calculations with account of spin-orbit coupling of phonon dispersion along three high-symmetry directions (Figure 3). For corrugated 1ML-HgTe nanoplatelet the phonon dispersion was also previously calculated in paper [51]. However, the authors of paper [51] provide no details of the calculation. To verify the results of our DFPT-calculations of phonon dispersion curves, we also accomplished the corresponding calculations within the supercell finite displacement method [47] implemented in Phono3py code [49,50]. Besides, we studied the convergence of the results depending on the supercell extension for various displacements of ions and number of **k**-points in the irreducible part of the Brillouin zone. It turned out that the results were very sensitive to the selection of these calculation parameters, and imaginary frequencies in phonon dispersion disappear only upon achievement of supercell extension 5×5×1 and use of **k**-mesh 2×2×2. Our calculations of phonon dispersion for zigzag-like 1ML-HgTe nanoplatelet carried out by two different methods confirmed the pattern of phonon dispersion

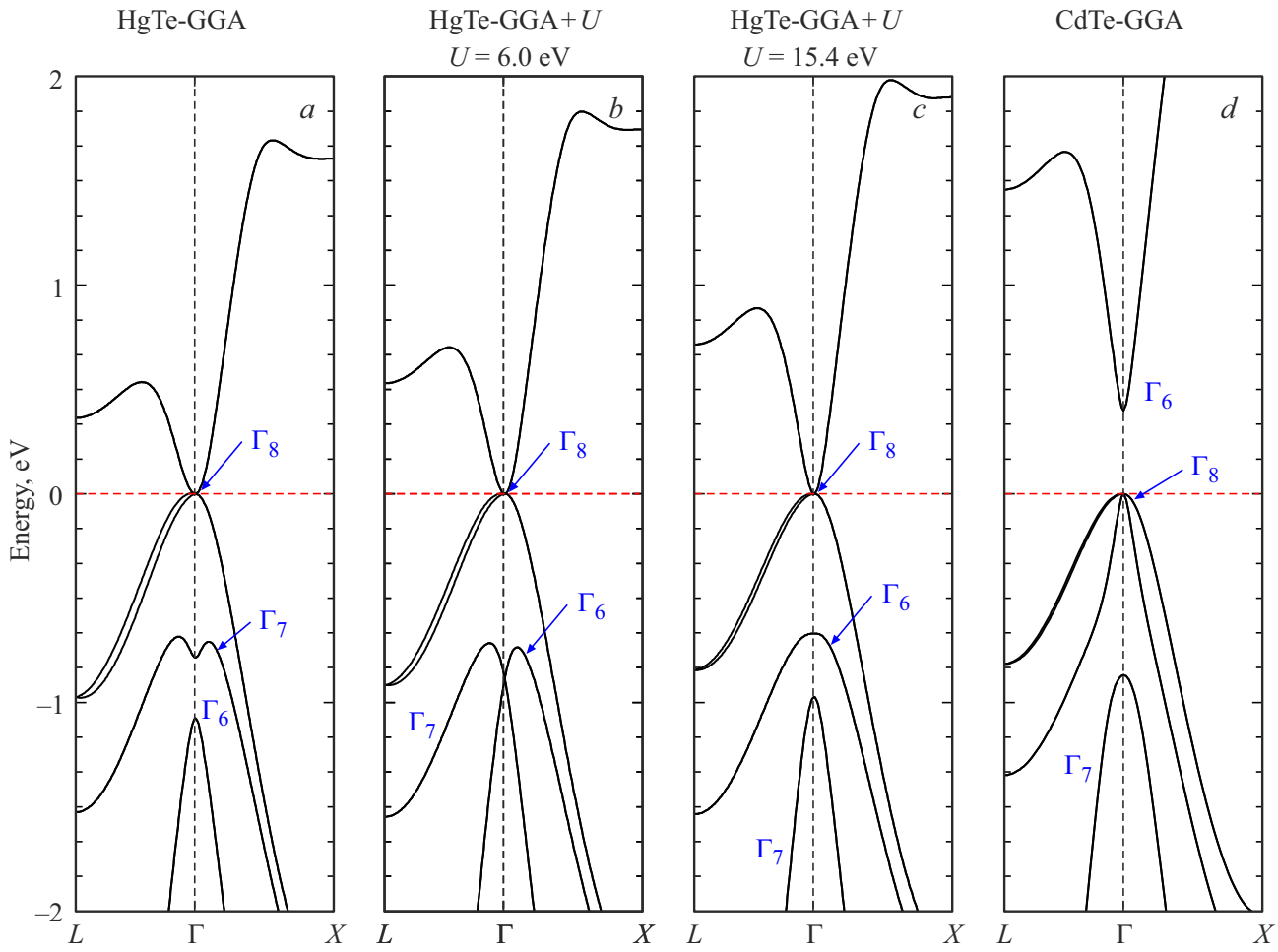

Figure 5. Band structures of crystals with zinc blende structure (sphalerite) calculated in GGA-approximation with exchange-correlation functional PBEsol with account of spin-orbit coupling: *a*) HgTe — GGA, *b*) HgTe — GGA+U at $U = 6.0$ eV, $J = 1.0$ eV, *c*) HgTe — GGA+U at $U = 15.4$ eV, $J = 1.0$ eV, *d*) CdTe — GGA.

obtained in paper [51]. As for the pattern of dispersion phonon branches for 2ML-HgTe nanoplatelet calculated in this paper, it also does not include imaginary frequencies (Figure 4). Therefore, our calculations of phonon dispersion both by DFPT method and supercell finite displacements method demonstrated thermodynamic stability of 1ML- and 2ML-HgTe nanoplatelets. It is important to note that the calculations of phonon spectra that we made for 1ML- and 2ML-HgTe nanoplatelets, but not taking into account the spin-orbit coupling, demonstrate the presence of imaginary frequencies. This means that the accounting of spin-orbit coupling in HgTe calculations is necessary not only to obtain the proper order of bands, but also for the thermodynamic stability of HgTe nanoplatelets.

Having confirmed the thermodynamic stability of 1ML- and 2ML-HgTe nanoplatelets, we then performed DFT-calculations with account of spin-orbit coupling of band structures of both nanoplatelets as well as bulk HgTe. The states were classified according to irreducible representations of a double point group C_{3v} (3m) for both nanoplatelets and a double point group T_d (-43m) for bulk HgTe with the zinc blende structure. For bulk HgTe and zigzag-like 1ML-HgTe monolayer, the calculations of band structure using DFT method were also carried out in paper [51]. However, the authors of the cited paper used the exchange-correlation functional in the local density approximation (LDA), as well as the modified Becke–Johnson (mBJ) potential [52]. It turned out that LDA functional causes the wrong order of bands Γ_6 and Γ_7 in the bulk HgTe, which is corrected using mBJ potential. The authors state, referring to paper [53], that the main reason for the wrong order of bands Γ_6 and Γ_7 of bulk HgTe in LDA-calculations is poor description of p−d-hybridization between semicore 5d-states of Hg and valence p-states of Te, which causes a shift in 5p-states of Te towards higher energies. The question of whether a semilocal functional of simpler form than mBJ can cause proper order of bands was left beyond the scope of paper [51]. To answer this question, we conducted DFT-calculations of the band structure of bulk HgTe with semilocal GGA-functional in the form of PBEsol [26]. It turned out that they, like calculations with local LDA-functional, also did not reproduce the

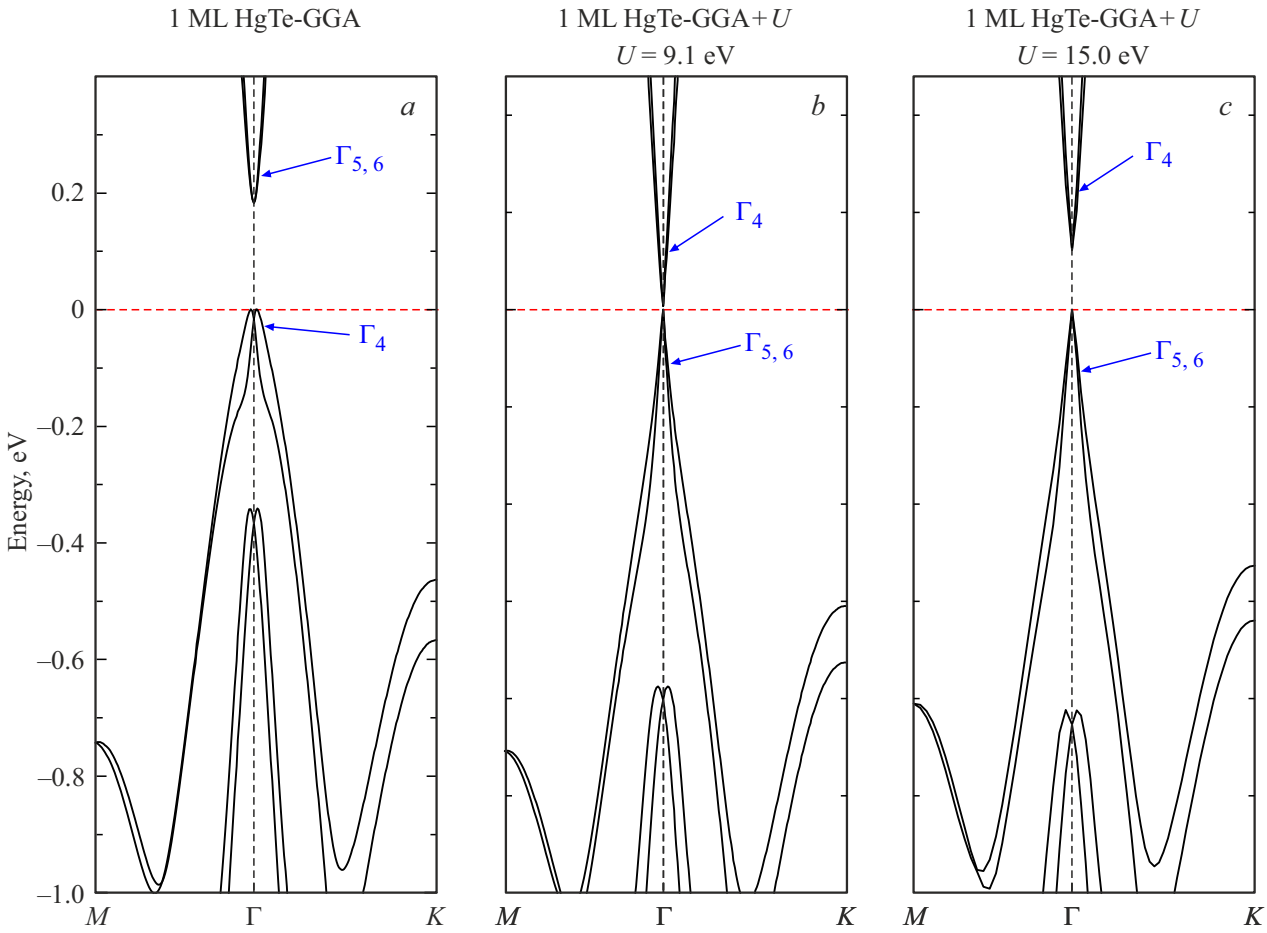

Figure 6. Band structures of 1ML-HgTe monolayer calculated in approximations *a*) GGA, *b*) GGA+U at $U = 9.1$ eV, $J = 1.0$ eV, *c*) GGA+U at $U = 15.0$ eV, $J = 1.0$ eV.

proper order of bands in bulk HgTe (see Figure 5, *a*). It is of interest to search for such methods of calculation that would enable one to reproduce the band order obtained in DFT-calculations of the band structure of bulk HgTe with mBJ functional, but simpler ones. Our attention was drawn to paper [54], which showed that the proper band order of *bulk* HgTe could be obtained taking into account the single-node repulsion of the Hg 5d-electrons within the GGA+U method.

Besides, to verify the calculation results with account of Hubbard repulsion in both formulations, we selected in our paper not the minimum value of U parameter, at which the proper band order appears, but the one at which the two-humped band Γ_6 becomes single-humped, as in reference calculations using mBJ functional [30].

In our paper the band structure calculations using GGA+U method carried out not only for the bulk HgTe, as in paper [54], but also for 1ML- and 2ML-HgTe nanoplatelets.

Figure 5, *a*–*c* shows band structures of bulk HgTe, calculated using DFT method with GGA exchange-correlation functional PBEsol and with account of spin-orbit coupling. In the band pattern of bulk HgTe (Figure 5, *a*) s-band Γ_6 is located below p-band Γ_7, which corresponds to the wrong order obtained in DFT-calculations in LDA and GGA approximations. When the Hubbard single-node interaction is added to the calculation, the nature of the band pattern of bulk HgTe changes: as U grows, the distance between the Γ_7 and Γ_6 bands in point Γ decreases, which happens down to values of $U = 6.0$ eV in Liechtenstein's model (with $J = 1.0$ eV) and $U = 5.0$ eV in Dudarev's model. Upon achievement of the specified „turning" values U, „gluing" and „flip" happen in point Γ of two bands Γ_7 and Γ_6: bands Γ_7 and Γ_6 change places, thus reproducing the band order (Γ_7–Γ_6–Γ_8) specific for inverse band structure of bulk HgTe as shown in Figure 5, *b*. With further increase of U the distance between bands Γ_7 and Γ_6 starts increasing, at the same time the band order remains proper (Figure 5, *c*). The difference in „turning" values of Hubbard parameter U in the Liechtenstein formulation in this paper and paper [54] is caused, in our opinion, by the fact that different GGA-functionals are used (PBEsol — in our paper and presumably PBE — in paper [54]). Figure 5, *d* shows for comparison the band structure of bulk CdTe, calculated in the same approximations as HgTe crystal, but without inclusion of Hubbard interaction. From Figure 5, *d* you

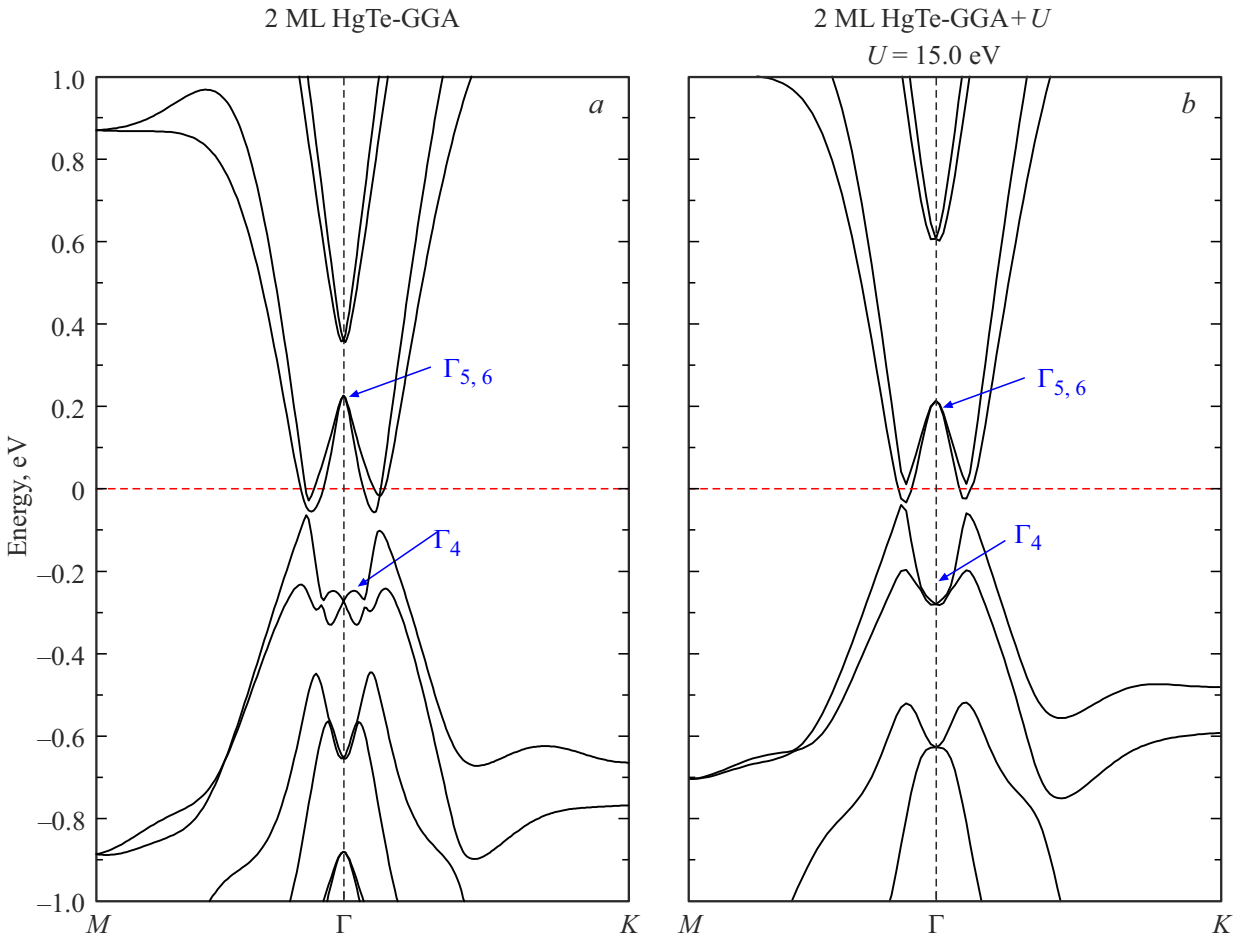

Figure 7. Band structures of 2ML-HgTe nanoplatelet calculated in approximations *a*) GGA, *b*) GGA+U at $U = 15.0$ eV, $J = 1.0$ eV.

can see that the band structure of bulk CdTe has band order $\Gamma_7-\Gamma_8-\Gamma_6$. At the same time the p-band Γ_7 occupies in the band pattern the same position as in the band pattern of bulk HgTe with the proper inverse order (Figure 5, *b* and *c*). The difference in band structures of CdTe and HgTe crystals consists in inversion of Γ_6 and Γ_8 bands and in the absence of energy gap in bulk HgTe.

Band structures of bulk HgTe, presented in Figure 5, *b* and *c*, are compliant with semimetal with inverse band order (p-band Γ_8 turns out to be higher than s-band Γ_6). Besides, p-bands Γ_8 of heavy and light holes are degenerate in the center of the Brillouin zone.

Apart from band structures of bulk HgTe, we also calculated band structures of 1ML and 2ML nanoplatelets. Band states of both nanoplatelets were classified according to irreducible representations of a double point group C_{3v} (3m) [55,56], which has 3 IRs, two one-dimensional Γ_5, Γ_6 and one two-dimensional Γ_4. Additional degeneracy $\left(E(\Gamma_5) = E(\Gamma_6)\right)$ in Figures 6 and 7 is caused by time reversal symmetry. For 1ML-HgTe monolayer the results of calculations were similar to those for the bulk one. Thus, GGA approximation does not reproduce the proper band order in point Γ: s-band Γ_4 turns out to be lower in energy than the p-bands $\Gamma_{5,6}$ (see Figure 6, *a*). (The same band order is obtained in paper [51] for zigzag-like 1ML-HgTe, calculated in LDA-approximation). Besides, in GGA-approximation the valence band of 1ML-HgTe monolayer has a two-humped structure in the vicinity of point Γ, and 1ML-HgTe is an indirect band gap semiconductor. When Hubbard interaction is added, the nature of the 1ML-HgTe band pattern changes: with growth of U the distance between bands Γ_4 and $\Gamma_{5,6}$ decreases down to values of $U = 9.1$ eV in the Liechtenstein's model ($J = 1.0$ eV). At the „turning" value of $U = 9.1$ eV the „gluing" and „flip" of bands occurs in point Γ, as shown in Figure 6, *b*. Besides, the order of Γ_4 and $\Gamma_{5,6}$ bands becomes proper, specific for the band structure obtained in paper [51] in the calculations with mBJ functional. With further growth of U the energy gap between Γ_4 and $\Gamma_{5,6}$ bands „opens" — 1ML-HgTe becomes a direct band gap semiconductor — grows slowly and reaches the value of 0.1 eV at $U = 15.0$ eV (see Figure 6, *c*).

Summing up, one can say that depending on the calculation method, the band structure of 1ML-HgTe nanoplatelet has either inverse or normal band order. The inverse order of bands is obtained in calculations within LDA and GGA

approximations, and the normal one — in calculations with mBJ functional, and also within GGA+U approximation, as shown in this paper.

Band structures of 2ML-HgTe nanoplatelet in sphalerite phase calculated using GGA and GGA+U functionals are presented in Figure 7. One can see that both approximations yield the same band order for 2ML-HgTe in point Γ — s-band Γ_4 turns out to be lower in energy than p-bands $\Gamma_{5,6}$. When Hubbard interaction is added, the 2ML-HgTe GGA band structure does not change dramatically (see Figure 7, *b*, which shows the band structure pattern for $U = 15.0$ eV, $J = 1.0$ eV). Note substantial differences in GGA+U band structures 1ML-HgTe and 2ML-HgTe (see Figure 6, *b, c* and 7, *b*). While 1ML-HgTe is a direct band gap semiconductor in point Γ, the 2ML-HgTe valence band has in the vicinity of Γ point the two maxima that are asymmetric relative to Γ: the left peak is slightly higher than the right one. Besides, such nature of the band structure 2ML-HgTe occus both in GGA-approximation and in GGA+U. Moreover, in contrast with the 1ML-HgTe band structure, having band order $\Gamma_4-\Gamma_{5,6}$, which in paper [51] was associated with a trivial insulator, the 2ML-HgTe band structure has the inverse band order $\Gamma_{5,6}-\Gamma_4$. I.e. as the thickness of HgTe nanoplatelet increases from one to two monolayers, the band order becomes inverse.

Near the Fermi level, the band structure of 2ML-HgTe plate, not having the center of inversion, shows similarity to the band structure specific for Weyl semimetal of II type [57]. You can confirm that if you refer to the sketch of the dispersion law $E(k)$ of a Weyl semimetal of type II, which represents two oppositely directed parabolas with axes of symmetry shifted relative to each other [58]. Inclined cones are formed at the intersection of these parabolas (of conduction band and valence band), and the cones are specific for a type II Weyl semimetal, which can be treated as a semiconductor with negative indirect band gap. The intersection points of parabolas are usually called Weyl nodes. However, the band diagram of 2ML-HgTe plate that we calculated (Figure 7) shows no the conduction and valence band intersection points. It can be explained qualitatively, if you take into account the Wigner–Neumann theorem [59], according to which the intersection of terms of the same symmetry is impossible [60]. In our calculation the states of the conduction and valence bands at the points of common position correspond to one and the same irreducible representation, and therefore the valence band and the conduction band are pushed apart in the vicinity of these points, which results in a diagram shown in Figure 7.

4. Conclusion

In this work, the electronic structure of mercury telluride in the sphalerite phase, both of bulk one and ultrathin 2D nanoplatelets 1ML-HgTe and 2ML-HgTe, was investigated using the plane-wave DFT method with account of spin-orbit coupling in the GGA and GGA+U approximations with the exchange-correlation functional in the form of PBEsol. By calculation of phonon dispersion, thermodynamic stability of HgTe nanoplatelets with thickness of 1ML and 2ML was established.

It was demonstrated that for mercury chalcogenide made of heavy elements, strong spin-orbit coupling in a combination with a two-dimensional quantum confinement causes significant changes in the electronic band structure of 2D nanoplatelets in the ultrathin limit and ordering of their boundary bands compared to the initial 3D-material.

It was shown that bulk HgTe, as it should have been expected, is a gapless semiconductor, the zigzag 1ML-HgTe nanoplatelet is a direct band gap at the Γ point semiconductor.

A whole series of interesting features in band structure of 2ML-HgTe nanoplatelet was discovered. As the thickness of nanoplatelet increases from one to two monolayers, the band order becomes inverse, and the energy gap „collapses“. In the vicinity of the Fermi level the valence band has two maxima near Γ point, which are asymmetric relative to Γ point, and the conduction band, accordingly, two minima. A similarity was revealed between the band structure of 2ML-HgTe plate near the Fermi level and the band structure specific for a type II Weyl semimetal. A qualitative explanation of this effect was given, which is related to the repulsion of states of the valence and conduction bands, having one and the same symmetry, in accordance with Wigner–Neumann theorem.

Acknowledgments

AVK is grateful to Herzen University for the support of this study within the internal grant № 43-VG; VGK performed the work within the state assignment of the Ministry of Education and Science of the Russian Federation (subject FFUG-2024-0042). Some calculations were carried out using a supercomputer of Ioffe Physical-Technical Institute. VGK would like to thank I.I. Tupitsyn for discussion of some issues.

Conflict of interest

The authors declare that they have no conflict of interest.

References

[1] K.S. Novoselov, A.K. Geim, S.V. Morozov, D. Jiang, Y. Zhang, S.V. Dubonos, I.V. Grigorieva, A.A. Firsov. Sci. **306**, *5696*, 666 (2004).
[2] M. Xu, T. Liang, M. Shi, H. Chen. Chem. Rev. **113**, *5*, 3766 (2013).
[3] A.L. Ivanovskii. Russ. Chem. Rev. **81**, *7*, 571 (2012).
[4] K. Takeda, K. Shiraish. Phys. Rev. B **50**, *20*, 14916 (1994).
[5] Y. Zhang, Y.-W. Tan, H.L. Stromer, P. Kim. Nature **438**, *7065*, 201 (2005).
[6] E. Durgun, S. Tongay, S. Ciraci. Phys. Rev. B **72**, *7*, 075420 (2005).

[7] S. Cahangirov, M. Topsakal, E. Aktürk, H. Şahin, S. Ciraci. Phys. Rev. Lett. **102**, *23*, 236804 (2009).
[8] H. Şahin, S. Cahangirov, M. Topsakal, E. Bekaroglu, E. Akturk, R.T. Senger, S. Ciraci. Phys. Rev. B **80**, *15*, 155453 (2009).
[9] C.-C. Liu, W. Feng, Y. Yao. Phys. Rev. Lett. **107**, *7*, 076802 (2011).
[10] B. Aufray, A. Kara, S. Vizzini, H. Oughaddou, C. Léandri, B. Ealet, G. Le Lay. Appl. Phys. Lett. **96**, *18*, 183102 (2010).
[11] B. Lalmi, H. Oughaddou, H. Enriquez, A. Kara, S. Vizzini, B. Ealet, B. Aufray. Appl. Phys. Lett. **97**, *22*, 223109 (2010).
[12] B. Feng, Z. Ding, S. Meng, Y. Yao, X. He, P. Cheng, L. Chen, K. Wu. Nano Lett. **12**, *7,* 3507 (2012).
[13] J. Sone, T. Yamagami, Y. Aoki, K. Nakatsuji, H. Hirayama. New J. Phys. **16**, *9*, 095004 (2014).
[14] L. Meng, Y. Wang, L. Zhang, S. Du, R. Wu, L. Li, Y. Zhang, G. Li, H. Zhou, W.A. Hofer, H.-J. Gao. Nano Lett. **13**, *2*, 685 (2013).
[15] A. Fleurence, R. Friedlein, T. Ozaki, H. Kawai, Y. Wang, Y. Yamada-Takamura. Phys. Rev. Lett. **108**, *24*, 245501 (2012).
[16] I.M. Tsidilkovskii. Besschelevye poluprovodniki — noviy klass veschestv. Nauka, M. (1986). 240 s. (in Russian).
[17] S.H. Groves, R.N. Brown, C.R. Pidgeon. Phys. Rev. **161**, *3*, 779 (1967).
[18] N. Orlowski, J. Augustin, Z. Gołacki, C. Janowitz, R. Manzke. Phys. Rev. B **61**, *8*, R5058(R) (2000).
[19] S. Murakami, N. Nagaosa, S.-C. Zhang. Phys. Rev. Lett. **93**, *15*, 156804 (2004).
[20] X.-L. Qi, Y.-S. Wu, S.-C. Zhang. Phys. Rev. B **74**, *8*, 085308 (2006).
[21] B.A. Bernevig, T.L. Hughes, S.-C. Zhang. Sci. **314**, *5806*, 1757 (2006).
[22] B.T. Diroll, B. Guzelturk, H. Po, C. Dabard, N. Fu, L. Makke, E. Lhuillier, S. Ithurria. Chem. Rev. **123**, *7*, 3543 (2023).
[23] V.G. Kuznetsov, A.A. Gavrikov, A.V. Kolobov. Mater. **16**, *23*, 7494 (2023).
[24] A.A. Gavrikov, V.G. Kuznetsov, A.V. Kolobov. Semiconductors **58**, *2*, 120 (2024).
[25] A.I. Ekimov, Al.L. Efros, A.A. Onushchenko. Solid State Commun. **56**, *11*, 921 (1985).
[26] J.P. Perdew, A. Ruzsinszky, G.I. Csonka, O.A. Vydrov, G.E. Scuseria, L.A. Constantin, X. Zhou, K. Burke. Phys. Rev. Lett. **100**, *13*, 136406 (2008).
[27] P. Giannozzi, S. Baroni, N. Bonini, M. Calandra, R. Car, C. Cavazzoni, D. Ceresoli, G.L. Chiarotti, M. Cococcioni, I. Dabo. J. Phys.: Condens. Matter **21**, *39*, 395502 (2009).
[28] P. Giannozzi, O. Andreussi, T. Brumme, O. Bunau, M. Buongiorno Nardelli, M. Calandra, R. Car, C. Cavazzoni, D. Ceresoli, M. Cococcioni, N. Colonna, I. Carnimeo, A. Dal Corso, S. de Gironcoli, P. Delugas, R.A. DiStasio Jr, A. Ferretti, A. Floris, G. Fratesi, G. Fugallo, R. Gebauer, U. Gerstmann, F. Giustino, T. Gorni, J. Jia, M. Kawamura, H.-Y. Ko, A. Kokalj, E. Küçükbenli, M. Lazzeri, M. Marsili, N. Marzari, F. Mauri, N.L. Nguyen, H.-V. Nguyen, A. Otero-de-la-Roza, L. Paulatto, S. Poncé, D. Rocca, R. Sabatini, B. Santra, M. Schlipf, A.P. Seitsonen, A. Smogunov, I. Timrov, T. Thonhauser, P. Umari, N. Vast, X. Wu, S. Baroni. J. Phys.: Condens. Matter **29**, *46*, 465901 (2017).
[29] A.I. Liechtenstein, V.I. Anisimov, J. Zaanen. Phys. Rev. B **52**, *8*, R5467(R) (1995).
[30] S.L. Dudarev, G.A. Botton, S.Y. Savrasov, C.J. Humphreys, A.P. Sutton. Phys. Rev. B **57**, *3*, 1505 (1998).
[31] P.E. Blöchl. Phys. Rev. B **50**, *24*, 17953 (1994).
[32] A. Dal Corso. Comput. Mater. Sci. **95**, 337 (2014).
[33] V. Eyert. J. Comput. Phys. **124**, *2*, 271 (1996).
[34] W.H. Press, B.P. Flannery, S.A. Teukolsky, W.T. Vetterling. Numerical Recipes in C. Cambridge University Press, Cambridge, UK (1992). 994p.
[35] D.F. Shanno. Math. Oper. Res.**3**, *3*, 244 (1978).
[36] B.G. Pfrommer, M. Côté, S.G. Louie, M.L. Cohen. J. Comput. Phys **131**, *1*, 233 (1997).
[37] H.J. Monkhorst, J.D. Pack. Phys. Rev. B **13**, *12*, 5188 (1976).
[38] S. Baroni, P. Giannozzi, A. Testa. Phys. Rev. Lett. **58**, *18*, 1861 (1987).
[39] X. Gonze, J.-P. Vigneron. Phys. Rev. B **39**, *18*, 13120 (1989).
[40] P. Giannozzi, S. de Gironcoli, P. Pavone, S. Baroni. Phys. Rev. B **43**, *9*, 7231 (1991).
[41] X. Gonze. Phys. Rev. A **52**, *2*, 1096 (1995).
[42] X. Gonze. Phys. Rev. A **54**, *5*, 4591 (E) (1996).
[43] X. Gonze. Phys. Rev. B **55**, *16*, 10337 (1997).
[44] S.Y. Savrasov. Phys. Rev. B **54**, *23*, 16470 (1996).
[45] X. Gonze, C. Lee. Phys. Rev. B **55**, *16*, 10355 (1997).
[46] S. Baroni, S. de Gironcoli, A. Dal Corso, P. Giannozzi. Rev. Mod. Phys. **73**, *2*, 515 (2001).
[47] K. Parlinski, Z.Q. Li, Y. Kawazoe. Phys. Rev. Lett. **78**, *21*, 4063 (1997).
[48] T. Sohier, M. Calandra, F. Mauri. Phys. Rev. B **96**, *7*, 075448 (2017).
[49] A. Togo, L. Chaput, T. Tadano, I. Tanaka. J. Phys.: Condens. Matter **35**, *35*, 353001 (2023).
[50] A. Togo. J. Phys. Soc. Jpn. **92**, *1*, 012001 (2023).
[51] J. Li, C. He, L. Meng, H. Xiao, C. Tang, X. Wei, J. Kim, N. Kioussis, G.M. Stocks, J. Zhong. Sci. Rep. **5**, *1*, 14115 (2015).
[52] F. Tran, P. Blaha. Phys. Rev. Lett. **102**, *22*, 226401 (2009).
[53] S.-H. Wei, A. Zunger. Phys. Rev. B **37**, *15*, 8958 (1998).
[54] J. Anversa, P. Piquini, A. Fazzio, T.M. Schmidt. Phys. Rev. B **90**, *19*, 195311 (2014).
[55] G.F. Koster, J.O. Dimmock, R.G. Wheeler, H. Statz. Properties of the Thirty-Two Point Groups. MIT Press, Cambridge, MA (1963). P. 55.
[56] V. Heine. Group Theory in Quantum Mechanics. Pergamon Press, London–Oxford–New York–Paris (1960).
[57] A.A. Soluyanov, D. Gresch, Z. Wang, Q.S. Wu, M. Troyer, X. Dai, A. Bernevig. Nature **527**, *7579*, 495 (2015).
[58] H. Zheng, M. Zahid Hasan. Adv. Phys. X **3**, *1*, 1466661 (2018).
[59] J. von Neumann, E. Wigner. Physik. Z. **30**, 465 (1929).
[60] L.D. Landau and E.M. Lifshitz, Kvantovaya mekhanika (nerelyativistskaya teoriya). Fizmatlit, M., (2004). S. 372. (In Russian).

Translated by M.Verenikina